Numerical dynamos

Caroline Nore
caroline.nore@limsi.fr

LIMSI-CNRS, University Paris-Sud, University Paris-Saclay, Orsay, France

Special thanks to the SFEMaNS team: L. Cappanera (Texas A & M), D. Castanon-Quiroz (Texas A & M), J.-L. Guermond (Texas A & M), J. Commenge (LIMSI), W. Herreman (LIMSI), F. Luddens (LM Raphael Salem, Rouen), J. Léorat (LUTH, Meudon), R. Laguerre (Obs. Royal de Belgique), A. Ribeiro (University California), K. Boronska (project manager, IBM, Wrocław)

July 27, 2016

Outline

Outline

1. Introduction

2. Overview of the numerical methods
   - 1D or 2D models
   - 3D periodic Cartesian geometry
   - Two periodic directions
   - Two periodic directions with vacuum
   - Sphere
   - Finite domains

3. Numerical models for von Kármán Sodium dynamo (VKS)
   - First step: periodic cartesian geometry and nonlinear codes
   - Second step: axially periodic cylindrical and kinematic code
   - Third step: finite cylinder and kinematic code
   - Fourth step: alpha-VKS in kinematic code
   - Fifth step: Direct Numerical Simulation

4. Conclusion

MHD equations

MHD (magnetohydrodynamics)

Interaction between electrically conducting fluid and magnetic field

The non-dimensionalised MHD equations:

- Navier-Stokes equations for an incompressible fluid:
$$\begin{aligned} \partial_t \mathbf{u} + \mathbf{u}\cdot\nabla\mathbf{u} - \frac{1}{R_e}\Delta\mathbf{u} + \nabla p &= (\nabla\times\frac{\mathbf{B}}{\mu_r})\times\mathbf{B} + \mathbf{f}, \\ \nabla\cdot\mathbf{u} &= 0. \end{aligned}$$
- Maxwell equations for the induction field $\mathbf{B}$ (magnetic field $\mathbf{H} = \mathbf{B}/\mu_r$):
$$\begin{aligned} \partial_t \mathbf{B} &= -\frac{1}{R_\mathrm{m}}\nabla\times\left(\frac{1}{\sigma_r}\nabla\times\frac{\mathbf{B}}{\mu_r}\right) + \nabla\times(\mathbf{u}\times\mathbf{B}), \\ \nabla\cdot\mathbf{B} &= 0. \end{aligned}$$
- Kinetic and magnetic Reynolds numbers with ν kinematic viscosity, μ_0 vacuum magnetic permeability, σ_0 fluid electrical conductivity (and magnetic Prandtl number):
$$R_e = \frac{U_\mathrm{ref}L_\mathrm{ref}}{\nu}, \qquad R_\mathrm{m} = \mu_0\sigma_0 U_\mathrm{ref}L_\mathrm{ref}, \qquad P_m = \frac{R_\mathrm{m}}{R_\mathrm{e}} = \mu_0\sigma_0\nu = \frac{\nu}{\eta}.$$
- Initial conditions (depend on the problem) and boundary conditions (BC)

Dynamo action

Boundary conditions in MHD

- kinematic BC for a fluid domain Ω of frontier Γ ($\mathbf{n}$ outward unit normal on Γ):
  - no-slip: $\mathbf{u}_{|\Gamma} = 0$
  - impenetrable BC: $\mathbf{n}\cdot\mathbf{u}_{|\Gamma} = 0$ and stress-free BC: $(\mathbf{n}\cdot\epsilon(\mathbf{u}))\times\mathbf{n}_{|\Gamma} = 0$ with the strain rate tensor $\epsilon(\mathbf{u}) := \frac{1}{2}\left(\nabla\mathbf{u} + \nabla\mathbf{u}^T\right)$.
- magnetic BC, transmission conditions (more difficult to impose in general):
  - at the frontier between 2 domains (conducting or insulating): $\mathbf{E}_1\times\mathbf{n}_1 + \mathbf{E}_2\times\mathbf{n}_2 = 0$ and $\mathbf{H}_1\times\mathbf{n}_1 + \mathbf{H}_2\times\mathbf{n}_2 = 0$ (resp. $\Rightarrow \mathbf{B}_1\cdot\mathbf{n}_1 + \mathbf{B}_2\cdot\mathbf{n}_2 = 0, \mathbf{j}_1\cdot\mathbf{n}_1 + \mathbf{j}_2\cdot\mathbf{n}_2 = 0$)
  - perfect conductor $\sigma_r \to \infty$ in contact with normal conductor ($\mathbf{n}^c$): $\mathbf{E}^c\times\mathbf{n}^c = 0 \Leftrightarrow \mathbf{j}^c\times\mathbf{n}^c = 0$ and $\mathbf{B}^c\cdot\mathbf{n}^c = 0$. Surface current: $\mathbf{H}^c\times\mathbf{n}^c = \mathbf{j}_s$
  - perfect ferromagnetic material (also called pseudo-vacuum or VTF Vanishing Tangential Field) $\mu_r \to \infty$ in contact with normal conductor: $\mathbf{H}^c\times\mathbf{n}^c = 0$ and $\mathbf{j}^c\cdot\mathbf{n}^c = 0$.

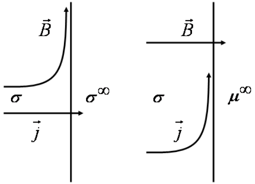

Dynamo action

We have a dynamo when the magnetic field is sustained: magnetic energy does not tend to 0 when time $\to \infty$ for some value of R_m

- $\mathbf{B} = 0$ is solution of MHD equations. Dynamo action when $\mathbf{B} = 0$ unstable, *i.e.* when $R_\mathrm{m} > R_\mathrm{m}^c(R_e, \mu_r, \sigma_r)$
- no dynamo theorem, some anti-dynamo theorems (Cowling's[1])
- kinematic problem: given a flow $\mathbf{u}$ (analytical $\mathbf{u}(\mathbf{x}, t)$, measurements, Navier-Stokes computation), how fast does the magnetic energy grow? Linear, eigenvalue problem - lots of theory, clean issues
- dynamical problem: given a mechanism for driving a flow (convection, shear, impellers) how does the field grow and saturate? Nonlinear, chaotic, issues of (MHD) turbulence. Usually requires numerical treatment - little theory

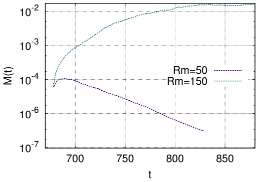

[1] An axisymmetric magnetic field vanishing at infinity cannot be maintained by dynamo action.

Dynamo action

full MHD equations with linear (Lorentz force neglected) and nonlinear regimes: parameter space $\{R_e, R_\mathrm{m}, \mu_r, \sigma_r\}$.

- onset of dynamo action monitored by the total magnetic energy, $M(t) = \frac{1}{2}\int_\Omega \mathbf{H}(\mathbf{r},t)\cdot\mathbf{B}(\mathbf{r},t)d\mathbf{r}$
- linear dynamo action $M(t) \approx \exp((\lambda_r + i\lambda_i)t)$ with $\lambda_r > 0$. Threshold $R_\mathrm{m} = R_\mathrm{m}^c(R_e, \mu_r, \sigma_r)$ when $\lambda_r = 0$.
- nonlinear dynamo action when $M(t)$ saturates. Question about mean energy partition $\frac{B^2}{\mu_0} = \rho V^2 f(R_e, R_\mathrm{m}, \mu_r, \sigma_r)$
- power needed to drive a turbulent flow $P \approx \rho U_{\mathrm{ref}}^3 L_{\mathrm{ref}}^3 / l_f = \rho\eta^3 R_\mathrm{m}^3 / l_f$

$\Rightarrow$ Interplay between analytical, experimental and numerical approaches.

Progress made thanks to numerics even if numerical limitations force to run codes at parameters far from realistic values: bad job in modeling the very small-scale flow dynamics but hopefully capture the larger-scale dynamo process correctly $\longrightarrow$

From simple to complex numerical computations

Outline

1D or 2D models

Ponomarenko dynamo (1973)

$\partial_t \mathbf{B} = -\frac{1}{R_\mathrm{m}} \nabla\times \left(\frac{1}{\sigma_r} \nabla\times \frac{\mathbf{B}}{\mu_r} \right) + \nabla\times(\mathbf{u}\times\mathbf{B})$, kinematic dynamo

- 1D2C axisymmetric rigid screw flow surrounded by conductor: $\mathbf{u}(r) = r\Omega\mathbf{e}_\theta + \chi r_0 \Omega \mathbf{e}_z$ for $r < r_0$ and $\mathbf{u} = 0$ for $r \geq r_0$. Kinetic helicity is $\mathcal{H}_\mathcal{K} = \mathbf{u}\cdot\nabla\times\mathbf{u} = 2\Omega^2 \chi r_0$
- discontinuity of $\mathbf{u}$ at $r = r_0$ (in conductor) provides strong shearing. Mechanism: stretching of radial field, diffusion of toroidal/azimuthal field and coupling through diffusion
- magnetic Reynolds number $R_\mathrm{m} = \mu_0 \sigma r_0^2 \Omega \sqrt{1+\chi^2}$ based on maximum velocity
- solution of the form $\mathbf{B} = \mathbf{b}(r)\exp[(\lambda_r + i\lambda_i)t + im\theta + ikz]$. The threshold is when $\lambda_r = 0$
- analytical optimization and matlab give $R_\mathrm{mc} = 17.7221, kr_0 = -0.3875, m = 1, \chi = 1.3141, r_0^2 \lambda_i \mu_0 \sigma = -0.4103$
- comparison with SFEMaNS using Kaiser and Tilgner (1999) parameters: pitch $\chi = 1$, periodic length $k = 2\pi/8$ and $R_\mathrm{m} = \mu_0 \sigma r_0^2 \Omega$, conducting domain $0 \leq r \leq r_1 \Rightarrow$
  - rotating magnetic field generated by shear near $r = r_0$
  - same scale for $\mathbf{u}$ and $\mathbf{B}$

1D or 2D models

Ponomarenko dynamo with SFEMaNS (Laguerre *et al.*, Proc. ULB, CTR, 2005)

- mechanism: stretching of radial field, diffusion of toroidal field and coupling through diffusion
- rotating magnetic field localized at discontinuity r_0
- same scale for $\mathbf{u}$ and $\mathbf{B}$

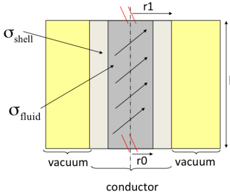

periodical box

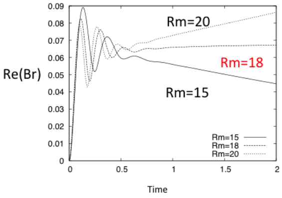

Time evolution of $\mathbf{B}$

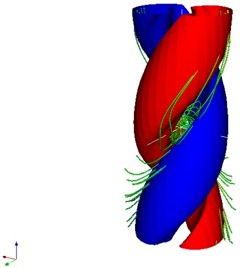

$R_{\mathrm{mc}}(=\mu_0 \sigma r_0^2 \Omega) \approx 18$ for discontinuous $\mathbf{u}$

1D or 2D models

Screw or spiral Couette dynamo (Dobler, Shukurov and Brandenburg, PRE 2002)

- smooth Ponomarenko profile created by spiral Couette flow (vertical velocity W_1 inside, angular velocity Ω_2 outside)
- 1D eigenvalue code and 3D periodic compressible code ($Mach < 0.5$), perfect conductor BC at R_2
- growth rate λ_r as a function of R_m: scaling laws as $R_\mathrm{m}^{-1/3}$ (like Ponomarenko case) and $R_\mathrm{m}^{-1/2}$: $\lambda_r \to 0$ as $R_\mathrm{m} \to \infty$ (slow dynamo)

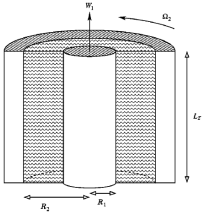

inner cylinder translates at W_1, outer cylinder rotates at Ω_2

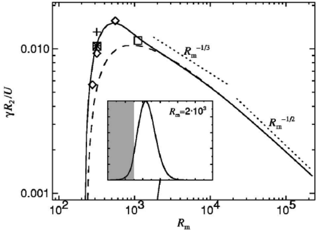

$\lambda_r(m = 1)$ vs R_m and radial magnetic energy profile for $0 \leq r \leq R_2$

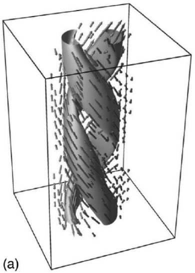

isosurface $|\mathbf{B}|$ 65% maximum at $R_e = 111$, $R_\mathrm{m} = 1110 > R_\mathrm{mc} \approx 218$

1D or 2D models

Riga experiment (Gailitis *et al.*, PRL, 2000)

optimization (Gailitis, Stefani, Dobler, Frick): $R_{\mathrm{mc}} = 10.8$

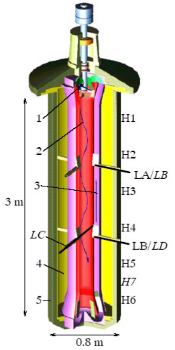

device with liquid sodium

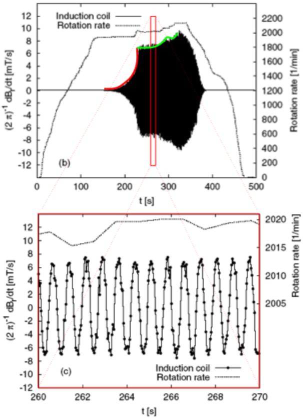

linear and saturated regimes

Rotating $m = 1$ mode $\Rightarrow$ two helices of opposite chirality with respect to $\mathbf{u}$

$\Rightarrow$ first evidence of an experimental fluid dynamo

1D or 2D models

Perm experiment

1D geometry to toroidal geometry with Perm experiment: the $m = 3$ mode is critical with $R_{\mathrm{mc}}(\textit{torus}) = 17.5$ and $R_{\mathrm{mc}}(\textit{Perm}) = 16$ (against $R_{\mathrm{mc}}(\textit{Pono}) = 10.8$)

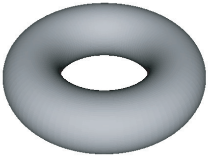

torus geometry

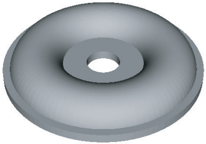

Perm geometry

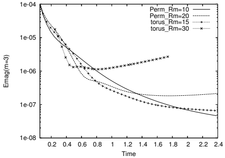

Magnetic energy $m = 3$

$t = 1$

$t \simeq 1 + \frac{1}{4} T_{\text{period}}$

Perm dynamo by SFEMaNS at $R_{\mathrm{m}} = 17$: iso-surfaces of the H_θ component of the $m = 3$ mode: 25% of the minimum (black) and of the maximum values (white)

1D or 2D models

Perm experiment

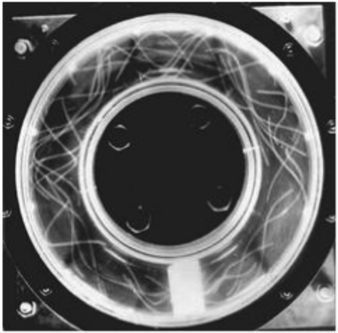

Torus in alloy based on copper on a turntable with diverters inside. Store kinetic energy in spinning torus and brake abruptly (within $0.1 - 0.2s$). Flow diverters make flow helical $\Rightarrow$ screw dynamo. Numerical results (Dobler, Frick and Stepanov, PRE 2003): field generation within $\leq 1s$, then decay of $\mathbf{B}$ and $\mathbf{u}$ but dynamo in the lab?

1D or 2D models

G.O. Roberts dynamo (1970)

$\partial_t \mathbf{B} = -\frac{1}{R_\mathrm{m}} \nabla\times \left(\frac{1}{\sigma_{\boldsymbol{r}}} \nabla\times \frac{\mathbf{B}}{\mu_{\boldsymbol{r}}} \right) + \nabla\times(\mathbf{u}\times\mathbf{B})$, kinematic dynamo

- 2D3C flow, independent of z but has a z-component
  $\mathbf{u} = (\cos y, \sin x, \sin y + \cos x) = (\partial_y \psi, -\partial_x \psi, \psi)$ with $\psi = \sin y + \cos x$.
  Special case of ABC (Arno'ld, Beltrami, Childress) flows
  $\mathbf{u} = (A \sin z + C \cos y, B \sin x + A \cos z, C \sin y + B \cos x)$. Beltrami flow s.t.
  $\nabla\times\mathbf{u} = \mathbf{u}$
- solution of the form $\mathbf{B} = \mathbf{b}(x, y, k)\exp(pt + ikz)$. Double Fourier series expansion for solving $\mathbf{b}(x, y, k)$
- steady helicoidal right-handed growing magnetic field at large scale:
  $\mathbf{B} = (-\sin kz, \cos kz, 0)\exp(pt)$. Different scales for $\mathbf{u}$ (small) and $\mathbf{B}$ (large)
- DNS by Ponty and Plunian, PRL 2011, transition from Large-Scale to Small-Scale dynamo
- Karlsruhe experiment

1D or 2D models

G.O. Roberts dynamo (Plunian, Rädler, Magnetohydrodynamics 2002)

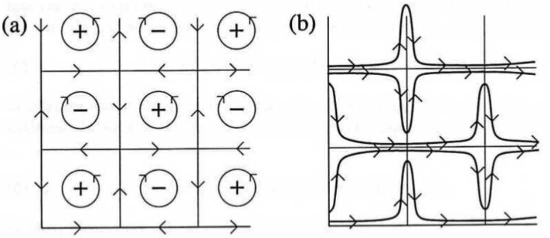

figure rotated through 45°: streamlines of $\mathbf{u}$ (left), $\mathbf{B}$ (right)

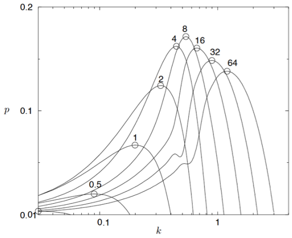

growth rate $p \sim \alpha k - k^2/R_\mathrm{m}$ at different R_m

- alternate helical loops (helicity) for $\mathbf{u}$
- steady helicoidal right-handed $\mathbf{B}$ field ($m = 1$ mode)
- at large R_m, generated field is expelled into boundary layers $\Rightarrow$ enhanced diffusion, leading to lower growth rates and ultimately to decay: $p \to 0$ as $R_\mathrm{m} \to \infty$ (slow dynamo)

1D or 2D models

G.O. Roberts dynamo (Ponty, Plunian, PRL 2011)

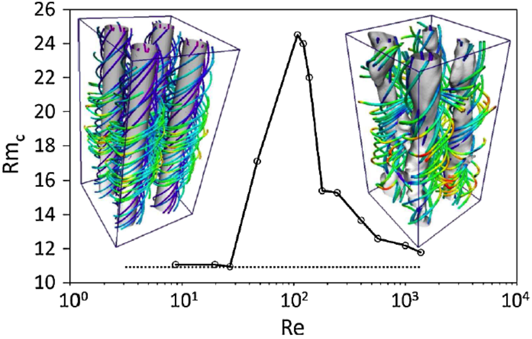

R_{mc} vs R_e, inset: **u** streamlines and time-averaged ω_z (laminar-left, turbulent-right)

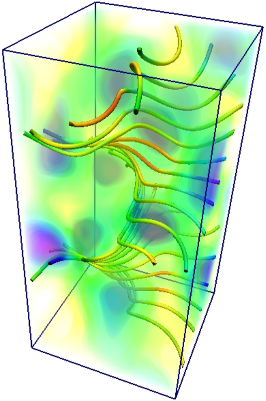

B streamlines

1D or 2D models

Karlsruhe dynamo experiment (Stieglitz, Muller, PoF, 2001)

52 helical loops with liquid sodium ⇒ second evidence of an experimental fluid dynamo

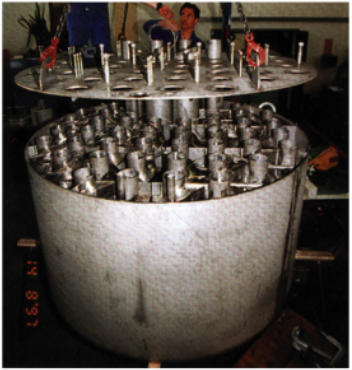

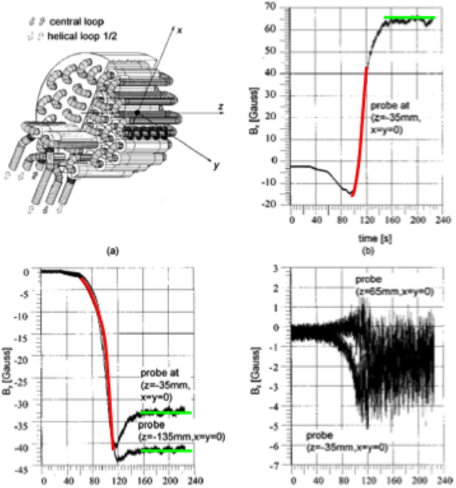

Overview of the numerical methods

3D periodic Cartesian geometry

- Essence of pseudo-spectral methods (Orszag, 1969): all differentiating done in spectral space, all multiplication in physical space. The key is the Fast Fourier Transform (FFT). Linear terms treated in spectral space, nonlinear terms in real space, and FFT used to go back and forth between physical and spectral spaces. Advance in time in spectral space. For incompressible Navier-Stokes equations, the pressure is eliminated by applying the divergence free operator in Fourier space.
- Examples of flows (no vacuum)
  - ABC-Arno'ld, Beltrami, Childress flow (Galanti, Sulem, Pouquet, GAFD 1992, Arnold, Galloway, Frisch)
    $\mathbf{u} = (A \sin z + C \cos y, B \sin x + A \cos z, C \sin y + B \cos x)$.
  - Taylor-Green flow (Brachet *et al.*, JFM 1983, Pouquet, Politano, Mininni, Ponty, Laval, Krstulovich)
    Simplest driving force in Navier-Stokes equations with constant velocity
    $\mathbf{f}(t) = f(t)\mathbf{v}^{TG}$ with $f(t)$ s.t. the (k_0, k_0, k_0) Fourier mode is constant
    $\mathbf{v}^{TG} = (\sin(k_0 x)\cos(k_0 y)\cos(k_0 z), -\cos(k_0 x)\sin(k_0 y)\cos(k_0 z), 0)$. Other ways: constant force (*i.e.* add $\mathbf{f}$ at each time-step) or constant injection power. Several symmetries are dynamically compatible and can increase the CPU efficiency (see later).

Overview of the numerical methods

Two periodic directions

Rotation-shear driven dynamo in an accretion disc **(Lesur, Fromang, Papaloizou, etc)**

- accretion discs found around young stars and compact objects
- gas spirals on the central object with outward turbulent transport of angular momentum
- discs may be turbulent due to the magnetorotational instability (MRI) **(Balbus, Hawley, 1991)**
- Focus on a small region of an accretion disc $\Rightarrow$ local model: incompressible Cartesian flow, with Ω local rotation and S linear radial shear:

$$\begin{aligned}
\partial_t \mathbf{u} + Sy\partial_x \mathbf{u} + \mathbf{u}\cdot\nabla\mathbf{u} &= -\nabla p - 2\Omega \mathbf{e}_z \times \mathbf{u} - Su_y \mathbf{e}_x + \mathbf{j}\times\mathbf{B} + \nu\Delta\mathbf{u}, \\
\partial_t \mathbf{B} + Sy\partial_x \mathbf{B} &= SB_y \mathbf{e}_x \nabla\times(\mathbf{u}\times\mathbf{B}) + \eta\Delta\mathbf{B}, \\
\nabla\cdot\mathbf{u} &= 0. \\
\nabla\cdot\mathbf{B} &= 0.
\end{aligned}$$

  where $\mathbf{u}, \mathbf{B}$ perturbations, with two cartesian periodic directions in z and $x(\phi)$ and shearing-periodic condition in $y(r)$ (no vacuum)

Rotation-shear driven disc dynamo (Lesur, Fromang, Papaloizou, etc)

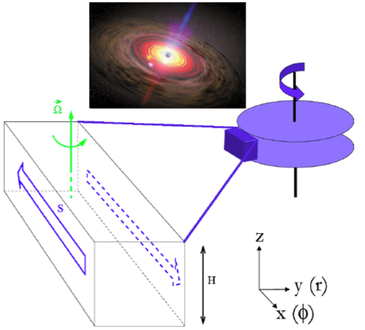

local model (shearing box). From Lesur, 2009

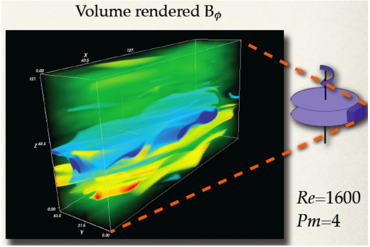

B_ϕ. From Lesur, 2009

- BC periodic in z and ϕ, shearing-periodic in r, no vacuum
- no averaged magnetic field (only generated by the flow)
- fast varying non axisymmetric structures involving a large scale $B_\phi(z)$
- dynamo starts for finite amplitude perturbations: transition to turbulence as a subcritical MHD instability

Overview of the numerical methods

BC with vacuum

- continuity of tangential components of $\mathbf{E}$ and $\mathbf{H}$
- continuity of normal component of $\mathbf{B} = \mu_0 \mu_r \mathbf{H}$ and $\mathbf{j}$
- if no jump in μ_r, continuity of $\mathbf{B} = \mu_0 \mathbf{H}$
- $\mathbf{j} = \nabla \times (\mathbf{B}/\mu_0) = 0$ in vacuum. If vacuum simply connected, $\mathbf{B}^v = \nabla \phi$ with $\nabla \cdot \mathbf{B} = 0 \Rightarrow \Delta \phi = 0$ (ϕ harmonic function).
  Depending on the geometry, we can have analytical solutions in vacuum:
  - plane layer: $\mathbf{B}^v \sim e^{\pm kz}$
  - infinite/axially periodic cylinder: $\mathbf{B}^v$ as Bessel functions in r
  - sphere: $\mathbf{B}^v$ as spherical harmonics in θ, φ
  - other: none

Overview of the numerical methods

Two periodic directions with vacuum

Convection driven plane layer dynamo (Cattaneo, Hughes, 2006)

Horizontal plane layer bounded between $z = \pm 0.5d$. Gravity and rotation axis in $\mathbf{e}_z$ direction, though sometimes have rotation axis tilted. Heated from below, usually with constant temperature on boundaries. Electrically insulating outside fluid layer. No-slip or stress-free boundaries.

$$
\begin{aligned}
\partial_t \mathbf{u} + \mathbf{u}\cdot\nabla\mathbf{u} + 2\Omega\mathbf{e}_z \times \mathbf{u} &= -\nabla p + \mathbf{j}\times\mathbf{B} + g\alpha T\mathbf{e}_z + \nu\Delta\mathbf{u}, \\
\partial_t \mathbf{B} &= \nabla\times(\mathbf{u}\times\mathbf{B}) + \eta\Delta\mathbf{B}, \\
\partial_t T + \mathbf{u}\cdot\nabla T &= \kappa\Delta\mathbf{T} + S_T, \\
\nabla\cdot\mathbf{u} &= 0. \\
\nabla\cdot\mathbf{B} &= 0.
\end{aligned}
$$

Use toroidal-poloidal expansions (divergenceless $\mathbf{u}$ and $\mathbf{B}$)

$$
\begin{aligned}
\mathbf{u} &= \nabla\times(e\mathbf{e}_z) + \nabla\times\nabla\times(f\mathbf{e}_z) + U_x(z,t)\mathbf{e}_x + U_y(z,t)\mathbf{e}_y, \\
\mathbf{B} &= \nabla\times(g\mathbf{e}_z) + \nabla\times\nabla\times(h\mathbf{e}_z) + B_x(z,t)\mathbf{e}_x + B_y(z,t)\mathbf{e}_y,
\end{aligned}
$$

where $U_x(z,t), U_y(z,t), B_x(z,t), B_y(z,t)$ mean parts . Take z-components of curl and curl curl of NS and z-components of induction eqn and its curl.

Convection driven plane layer dynamo (Cattaneo, Hughes, 2006)

Pseudo-spectral method with no-slip BC at $z = \pm 0.5$ $(\gamma = \beta = 2\pi)$:

$$f(x,y,z,t) = \sum_{l=-N_x+1}^{N_x} \sum_{m=-N_y+1}^{N_y} \sum_{n=1}^{N_z+2} f_{lmn}(t) e^{i(l\gamma x + m\beta y)} T_{n-1}(2z) \text{ or}$$

with stress-free BC with

$$f(x,y,z,t) = \sum_{l=-N_x+1}^{N_x} \sum_{m=-N_y+1}^{N_y} \sum_{n=1}^{N_z+2} f_{lmn} e^{i(l\gamma x + m\beta y)} \sin(n\pi(z+0.5))$$

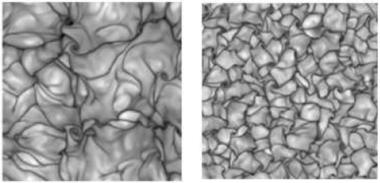

temperature, without or with rotation

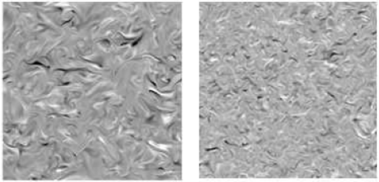

B_x, without or with rotation

Comparison between non-rotating (left) and rotating (right) cases at *Rayleigh* $\geq 5 \times 10^5$: light (dark) tones represent positive (negative) fluctuations

Overview of the numerical methods

Two periodic directions with vacuum

Dynamo in infinite cylinders

- cylinder $0 \leq r \leq R_{cyl}$: Bessel functions in r outside, pseudo-spectral in the azimuthal and axial directions, and compact finite differences in the radial direction inside (Léorat, 1994, Marié *et al.*, EPJB 2003, Ravelet *et al.*, PoF 2005)
- cylinder $R_1 \leq r \leq R_2$: Bessel functions in r outside, pseudo-spectral in the azimuthal and axial directions, and Chebychev expansion in the radial direction outside (Willis & Barenghi, JFM 2002)
  - toroidal-poloidal expansions in the conducting domain $R_1 \leq r \leq R_2$:
$$\begin{aligned}\mathbf{u} &= \psi_0(r,t)\mathbf{e}_\theta + \phi_0(r,t)\mathbf{e}_z + \nabla\times(\psi r\mathbf{e}_r) + \nabla\times\nabla\times(\phi_0 r\mathbf{e}_r),\\ \mathbf{B} &= \mathcal{T}_0(r,t)\mathbf{e}_\theta + \mathcal{P}_0(r,t)\mathbf{e}_z + \nabla\times(\mathcal{T} r\mathbf{e}_r) + \nabla\times\nabla\times(\mathcal{P} r\mathbf{e}_r),\end{aligned}$$
where $\psi_0, \phi_0, \mathcal{T}_0, \mathcal{P}_0$ are non-periodic parts and periodic parts are expanded as: $f(x,\theta,z,t) = \sum_{n=0}^{N} \sum_{|k|<K} \sum_{|m|<M} f_{nkm}(t) e^{i(\alpha kz + m_1 m\theta)} T_n(x)$ for $x \in [0,1], \theta \in [0, 2\pi/m_1], z \in [0, 2\pi/\alpha]$ $(r = R_1 + x(R_2 - R_1))$
  - $\mathbf{B} = \nabla\psi$ in the insulating domain (no j_θ imposed) $\Rightarrow \psi = R(r)\Theta(\theta)Z(z) = R(r)e^{i(m\theta + \alpha z)}$ with $R(r)$ solution of the modified Bessel functions. For $\alpha = 0$, $R(r) = r^{\pm m}$ for $r \leq R_1$ or $r \geq R_2$; for $\alpha \neq 0$, $R(r) = Im(\alpha r)$ for $r \leq R_1$ or $R(r) = Km(\alpha r)$ for $r \geq R_2$.

Overview of the numerical methods

Two periodic directions with vacuum

Example: Taylor-Couette dynamo (Willis & Barenghi, AA 2002)

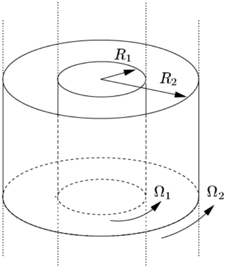

axially periodic cylinders

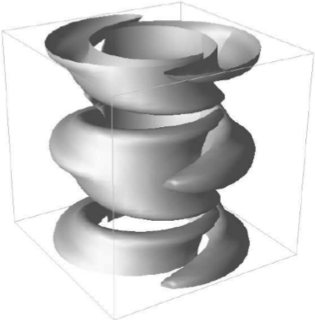

isosurface of $|\mathbf{B}|$ at $R_e = 120$, $R_{\mathrm{m}} = 240$

Figure : Self-consistent dynamo in axially periodic Taylor-Couette set-up with $R_1/R_2 = 0.5, \Omega_2 = 0$.

Larger scale for $\mathbf{B}$ than for $\mathbf{u}$ (Laure *et al.*, Nato Sci Ser. II 2000)

Overview of the numerical methods

Sphere

- kinematic dynamo: Dudley and James, Proc. Roy. Soc. London, 1989 (finite differences)
- nonlinear dynamo: use thermal convection and rotation as sources of motion
  - first 3D self-consistent Boussinesq models of thermal convection 20 yr ago (Glatzmaier and Roberts, Nature, 1995; Kageyama *et al.*, Nature, 1995), first milestones of modern dynamo modeling $\Rightarrow$ dipole excursions and reversals
  - benchmarks in spherical shell or full sphere: Christensen *et al.*, 2001; Christensen *et al.*, 2009; Jones *et al.*, 2011; Jackson *et al.*, 2013; Marti *et al.*, 2014; Matsui *et al.*, 2016 $\Rightarrow$ comparisons between pseudo-spectral and local methods, finite volume or finite element methods or mixed 'global-local' method (SFEMaNS)

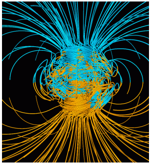

Magnetic field streamlines like a dipole and web page of G. Glatzmaier

Numerical methods for a sphere

- pseudo-spectral codes, usually with a poloidal–toroidal representation for magnetic field and velocity: spherical harmonic expansions in the angular variables and different approximations in r: **Chebyshev** polynomials (Tilgner, Busse, 1997; Hollerbach, 2000; Sasaki *et al.*, 2012, Simitev and Busse, 2014); **finite differences** (Sheyko, Marti and Jackson, 2014; Dormy in the code PARODY, Aubert in the code PARODY-JA; Schaeffer, 2012); **Worland polynomials** (Marti, Jackson, 2014)
- finite volume algorithm: magnetic and velocity fields directly; divergence-free condition for $\mathbf{B}$ implemented using a Lagrange multiplier; massively MPI-parallel unstructured finite-volume code, based on a domain decomposition with METIS (Vantieghem *et al.*, GJI 2016 with pseudo-vacuum BC)
- finite elements: magnetic and velocity fields directly; divergence-free condition for $\mathbf{B}$ implemented using a Lagrange multiplier; quadratic finite elements elements are used for $\mathbf{u}$, T and $\mathbf{B}$ and linear elements for P (Chan *et al.*, 2007).
- commercial code like COMSOL: finite elements for $\mathbf{u}, P, T$ and $\mathbf{A}$ (vector potential) (standard Lagrange element $\mathbb{P}_1$-$\mathbb{P}_2$-$\mathbb{P}_2$ for $P, \mathbf{u}, T$, quadratic edge elements for $\mathbf{A}$) (Cébron, 2014)

Overview of the numerical methods

Finite domains

- spheroid: dynamo in a precessional spheroid by Wu, Roberts, GAFD 2009 with Poincaré stress condition (problem, see Guermond *et al.*, EJMB 2013)
- torus: Morales *et al.*, PoP 2015 (using penalty method, see later)
- cylinder: Giesecke *et al.*, 2008–, Iskakov *et al.*, 2004, Nore *et al.*, 2006– (see VKS modeling)

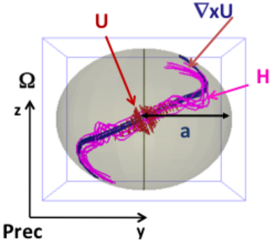

precessional spheroid

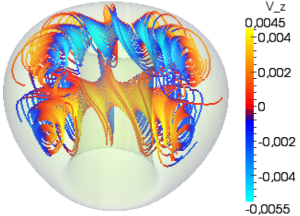

D-torus

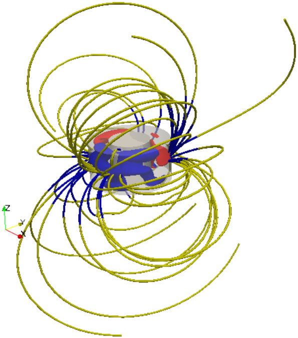

dynamo in a short Taylor-Couette cylinder

Outline

Motivation

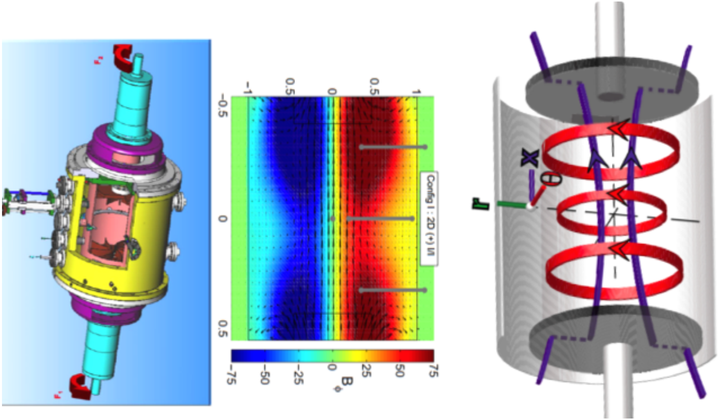

Figure : The von Kármán sodium experiment (VKS collaboration)

- mainly axisymmetric **B** (axial dipole and azimuthal component) for exactly counter-rotating impellers
- magnetic field generated only when impellers are made of soft iron with relative magnetic permeability $\mu_r > 1$. Why?

First step: periodic cartesian geometry and nonlinear codes

Taylor-Green vortex

$$\begin{aligned}\partial_t \mathbf{u} + \mathbf{u}\cdot\nabla\mathbf{u} &= -\nabla p + \mathbf{j}\times\mathbf{B} + \nu\Delta\mathbf{u} + \mathbf{f},\\ \partial_t \mathbf{B} &= \nabla\times(\mathbf{u}\times\mathbf{B}) + \eta\Delta\mathbf{B},\end{aligned}$$

with $\rho = 1$, $\nabla\cdot\mathbf{u} = 0, \nabla\cdot\mathbf{B} = 0$ and $\mathbf{f}(t) = f(t)\mathbf{v}^{TG}$ s.t. one keeps constant $\mathbf{v}^{TG} = (\sin(k_0 x)\cos(k_0 y)\cos(k_0 z), -\cos(k_0 x)\sin(k_0 y)\cos(k_0)z, 0)$. Plane $\mathbf{v}^{TG}$ not a dynamo but nonlinear $\mathbf{u}$ is 3D

Kinetic and magnetic Reynolds numbers as outputs: $R_e = \frac{U_{rms} L_{int}}{\nu}, R_\mathrm{m} = \frac{U_{rms} L_{int}}{\eta}$

with $U_{rms} = \overline{\sqrt{\langle \mathbf{u}^2 \rangle}}$ and $L_{int} = \int \frac{E(k)}{k} dk / \int E(k) dk$

with $\overline{f} = \int_0^T f(t)dt/T$, $\langle f \rangle = \int_{vol} f(\mathbf{x}) d^3\mathbf{x}/vol$

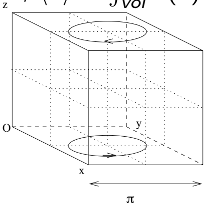

$k_0 = 1$ in the impermeable box $\{0, \pi\}^3$

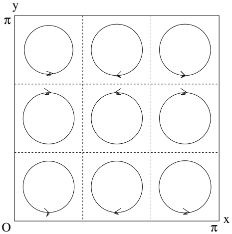

$k_0 = 3$

First step: periodic cartesian geometry and nonlinear codes

Taylor-Green vortex

Symmetries are dynamically compatible, *i.e.* IC as $\mathbf{v}^{TG}$ then solution $\mathbf{v}_s$ symmetric:

$$\begin{cases} v_{sx} = \sum_{m,n,p} \hat{u}_{sx}(m,n,p,t) \sin mx \cos ny \cos pz, \\ v_{sy} = \sum_{m,n,p} \hat{u}_{sy}(m,n,p,t) \cos mx \sin ny \cos pz, \\ v_{sz} = \sum_{m,n,p} \hat{u}_{sz}(m,n,p,t) \cos mx \cos ny \sin pz \end{cases}$$

where $\hat{u}_{sx}(m,n,p,t), \hat{u}_{sy}(m,n,p,t), \hat{u}_{sz}(m,n,p,t)$ vanish unless (m,n,p) are either all even or all odd integers + additional relations.

Corresponding rotational symmetries: of angle π around the axis $(x = z = \pi/2)$ and $(y = z = \pi/2)$; and of angle $\pi/2$ around the axis $(x = y = \pi/2)$. Planes of mirror symmetry: $x = 0, \pi$, $y = 0, \pi$, $z = 0, \pi$. Velocity parallel to these planes (impermeable box).

Different choices of symmetry for $\mathbf{B}$ and $\mathbf{j}$: Nore *et al.*, PoP 1997, $\mathbf{B}$ like $\mathbf{v}_s$ (perfect conductor), Krstulovic *et al.*, PRE 2013, multiple choices

First step: periodic cartesian geometry and nonlinear codes

Results (Nore *et al.*, PoP 1997)

early comparisons between a TG symmetric code and a general periodic code. Generation of magnetic field: slab mode with periodic code ($\sim$ equatorial dipole), use of scale separation for the TG symmetric code ($\mathbf{B}$ like $\mathbf{v}_s$, perfect conductor)

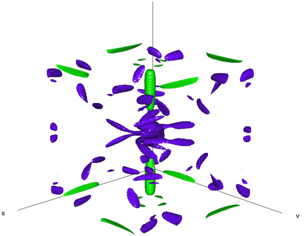

TG symmetric code $k_0 = 3$, isosurfaces of $\overline{B^2}$ (green) and ω^2 (purple), $R_e = 25$ and $R_\mathrm{m} = 44 > R_\mathrm{mc} \approx 40$ in $\{0, \pi\}^3$

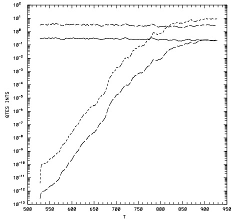

Periodic code with $k_0 = 1$, $\langle \boldsymbol{\omega}^2 \rangle, \langle \mathbf{u}^2 \rangle, \langle \mathbf{j}^2 \rangle, \langle \mathbf{B}^2 \rangle$ vs time

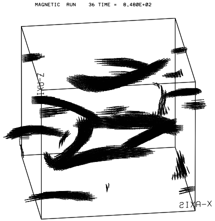

Periodic code $k_0 = 1$, vectors $\mathbf{B}$, $R_e = 10$ and $R_\mathrm{m} = 41 > R_\mathrm{mc} \approx 10$ in $\{0, 2\pi\}^3$

First step: periodic cartesian geometry and nonlinear codes

Results (Ponty *et al.*, NJP 2007, Dubrulle *et al.*, NJP 2007, Ponty, Laval *et al.*, PRL 2007)

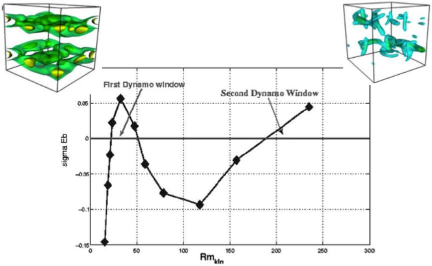

Growth rates for the kinematic dynamo generated by time-averaged flow versus R_{m} $\Rightarrow$ two dynamo branches: 1^{st} slab, 2^{nd} similar to equatorial $m = 1$ mode

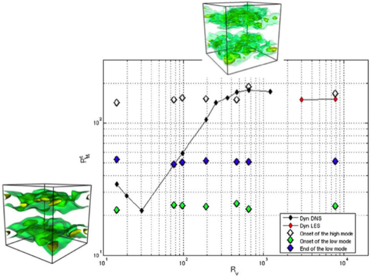

Evolution of R_{mc} for the kinematic runs from the time-averaged flow (diamond) and the dynamical runs in full line versus the Reynolds number R_e $\Rightarrow$ only slab mode

First step: periodic cartesian geometry and nonlinear codes

Results (Ponty *et al.*, NJP 2007, Dubrulle *et al.*, NJP 2007, Ponty, Laval *et al.*, PRL 2007)

hysteretic behavior due to hydrodynamic changes induced by the action of the Lorentz force

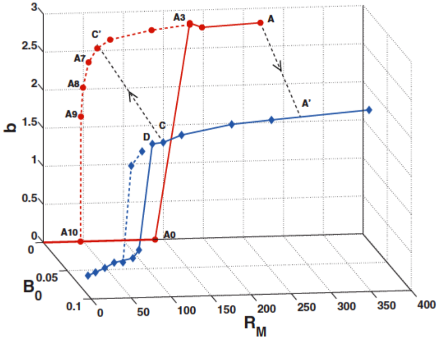

Bifurcation curves and hysteresis cycles when an external magnetic field is applied (diamond) or without one (circle)

First step: periodic cartesian geometry and nonlinear codes

Results (Krstulovic *et al.*, PRE, 2011)

use of mirror symmetries (*impermeable box*) for **u** and simplified BC for **B** $\rightarrow$ 6 distinct families of magnetic field: ICI, ICC, IIC, III, CCC, CCI where I is perfect ferromagnetic material and C is perfect conductor

- linear dynamo action at $R_e = 30$ (higher $R_{\rm mc}$ at $R_e = 150$):

Case	ICI	ICC	IIC	III	CCC	CCI
$R_{\rm mc}$	9	26	66	73	231	254

Table : Magnetic thresholds for $R_e = 30$

The III growing mode is an axial dipole ($P_m^c = 73/30 \approx 2.4$).

- nonlinear dynamo action for III case: super and sub-critical regimes due to hydrodynamic pitchfork bifurcation at $R_e = 22$. If following a line $R_{\rm m} = P_m R_e$, supercritical dynamo bifurcation for P_m large enough, subcritical for P_m small enough.

First step: periodic cartesian geometry and nonlinear codes

Linear and nonlinear dynamo action for III case

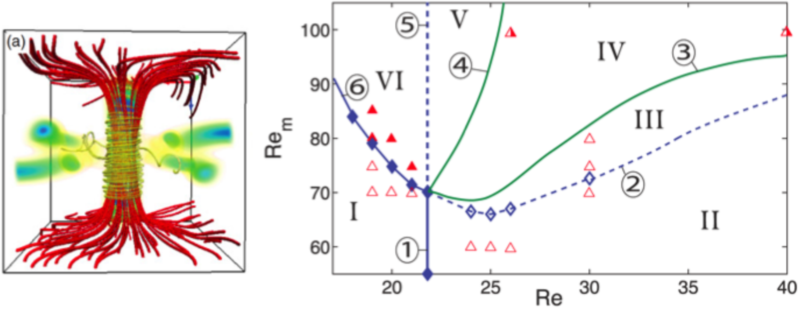

Figure : (a) **B** in red, **j** in yellow and density plot of highest magnetic energy zones of the growing mode at $R_{\mathrm{m}} = 80$ in $\{0, \pi\}^3$; (b) qualitative bifurcation diagram: blue for DNS, green for qualitative lines, filled (empty) triangles for a nonvanishing (vanishing) magnetic field at saturation, half-filled triangles for bistable zone

Similar to VKS dynamo for streamlines but not for localization of magnetic energy

Second step: axially periodic cylindrical and kinematic code

VKE flow

Use of the time and azimuthal-averaged flow VKE from a half-scale water experiment using LDV (small scales, non-axisymmetric and fluctuating perturbations filtered out): Cowling's thm $\Rightarrow$ $\mathbf{B}(m = 0)$ mode impossible
Numerical method pseudo-spectral in (θ, z) and finite differences in r, matching with exact solutions outside (Léorat AIAA, 1994).
Solution $\mathbf{B}(r, \theta, z, t) = \sum_{n,m} B_{n,m}(r, t) \exp(i(m\theta + nz))$
Symmetrized velocity field (Marié *et al.*, EPJB 2003, Ravelet *et al.*, PoF 2005)

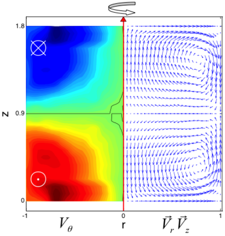

measured VKE

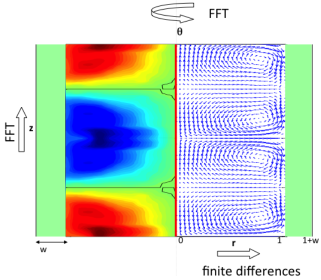

symmetrized VKE

Second step: axially periodic cylindrical and kinematic code

Results **(Ravelet *et al.*, PoF 2005)**

- optimization with different TM (TM28, TM73, TM60, etc)
- growing magnetic field is a $m = 1$ steady mode, equatorial dipole and two vertical structures aligned with the cylinder axis; compatible with Cowling's thm
- influence of the static side layers (same conductivity): R_{mc} decreases with w

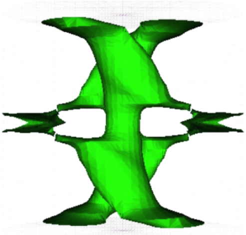

$w = 0$

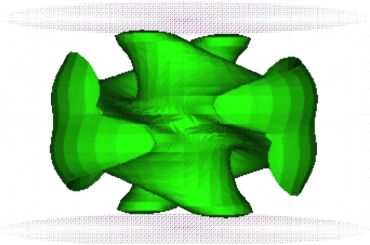

$w = 0.6$

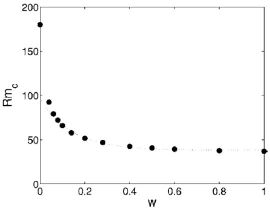

R_{mc} vs w

Third step: finite cylinder and kinematic code

MND[2] flow

MND flow for $0 \leq r \leq 1$ and $-1 \leq z \leq 1$:

$$v_r = -\frac{\pi}{2} r(1-r)^2(1+2r)\cos(\pi z),$$
$$v_\theta = 4\epsilon r(1-r)\sin(\pi z/2),$$
$$v_z = (1-r)(1+r-5r^2)\sin(\pi z).$$

$\epsilon = T/P = 0.7259$ (optimal value for the dynamo action)

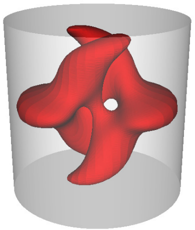

Figure : Kinematic $m=1$ mode with $w=0=l$ (vacuum) at $R_{\mathrm{m}} = 65 > R_{\mathrm{mc}} = 63.5$, SFEMaNS

Numerical methods

- Stefani, Xu (2004, Integral Equation Approach *IEA* [steady or time-dependent kinematic dynamos using Biot and Savart's law in conducting domain and BEM in vacuum], Differential Equation Approach *DEA*) same σ for fluid and wall
- Iskakov *et al.*, JCP 2004; Giesecke *et al.*, GAFD 2010 (FV-BEM code)
- SFEMaNS

[2] Marié, Normand, Daviaud, PoF 2006

Third step: finite cylinder and kinematic code

FV-BEM method

$$\partial_t \mathbf{B} = -\frac{1}{R_\mathrm{m}} \nabla \times \left(\frac{1}{\sigma_r} \nabla \times \frac{\mathbf{B}}{\mu_r} \right) + \nabla \times (\mathbf{u} \times \mathbf{B}) \text{ in the conducting domain}$$

$$\mathbf{B}^{n+1} = \mathbf{B}^n + \Delta t F^{\mathrm{exp}} \left[\mathbf{B}^n + \frac{\Delta t}{2} F[\mathbf{B}^n] \right] + \frac{\Delta t}{2} \left(F^{\mathrm{imp}}[\mathbf{B}^n] + F^{\mathrm{imp}}[\mathbf{B}^{n+1}] \right)$$

with **B** (resp. **E**) defined at the center of the cell face (resp. edge) and where explicit term $F^{\mathrm{exp}} \propto \nabla \times (\mathbf{u} \times \mathbf{B})$ and implicit term $F^{\mathrm{imp}} \propto \nabla \times (\eta \nabla \times \mathbf{B})$ and $F = F^{\mathrm{imp}} + F^{\mathrm{exp}}$

finite volume method: physical quantities are defined on a staggered mesh

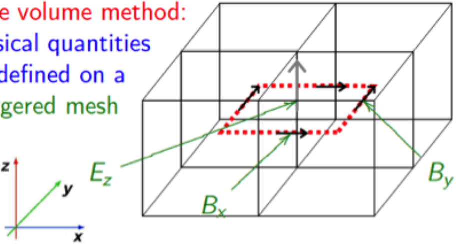

jump conditions

$$\mathbf{n} \cdot (\mathbf{B}_1 - \mathbf{B}_2) = 0$$

$$\mathbf{n} \times \left(\frac{\mathbf{B}_1}{\mu_{r,1}} - \frac{\mathbf{B}_2}{\mu_{r,2}} \right) = 0$$

$$\mathbf{n} \cdot (\sigma_1 \mathbf{E}_1 - \sigma_2 \mathbf{E}_2) = 0$$

$$\mathbf{n} \times (\mathbf{E}_1 - \mathbf{E}_2) = 0$$

Third step: finite cylinder and kinematic code

FV-BEM method

- procedure described in Iskakov, Descombes, Dormy, JCP 2004
- in a simply connected vacuum, $\nabla \times \mathbf{B} = 0 \Rightarrow \mathbf{B}$ can be expressed as the gradient of a scalar field Φ.

$$\mathbf{B} = -\nabla\Phi \quad \text{with} \quad \Delta\Phi = 0, \quad \Phi \to O(r^{-2}), r \to \infty$$

- Adopting Green's 2.theorem the integration of $\Delta\Phi = 0$ yields:

Boundary Integral Equation (BIE)

Γ : surface
$\mathbf{B}^{\mathrm{n}}$: normal component

$$\Phi(\mathbf{r}) = -2\int_{\Gamma}(\Phi(\mathbf{r}')\frac{\partial G(\mathbf{r},\mathbf{r}')}{\partial n} - \overbrace{\frac{\partial\Phi(\mathbf{r}')}{\partial n}}^{+B^{\mathrm{n}}(\mathbf{r}')} G(\mathbf{r},\mathbf{r}'))\mathrm{d}\Gamma(\mathbf{r}')$$

$G(\mathbf{r},\mathbf{r}')$: Greens-Function or fundamental solution

$$\Delta G(\mathbf{r},\mathbf{r}') = -\delta(\mathbf{r}-\mathbf{r}') \quad \Longrightarrow \quad G(\mathbf{r},\mathbf{r}') = -\frac{1}{4\pi\left|\mathbf{r}-\mathbf{r}'\right|}$$

Third step: finite cylinder and kinematic code

Surface discretization

- B^{n} is computed from FV-scheme
  $\Rightarrow$ compute Φ from BIE
  $\Rightarrow$ compute $B^{\tau} = -\hat{\mathbf{e}}_{\tau} \cdot \nabla \Phi$ used by FV
- discretisation: boundary element $\sim$ surface of a grid cell
- introduce global ordering scheme $i = 1 \ldots N$

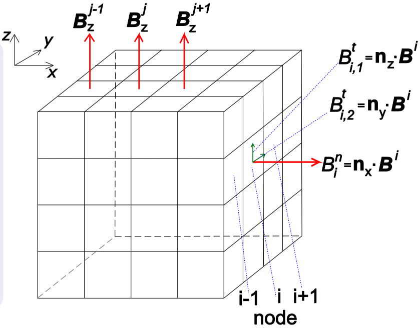

$$\frac{1}{2}\Phi_i = -\sum_j \underbrace{\left(\int_{\Gamma_j} \frac{\partial G}{\partial n}(\vec{r}_i, \vec{r}') \mathrm{d}\Gamma'_j \right)}_{\mathcal{A}_{ij}} \Phi_j - \sum_j \underbrace{\left(\int_{\Gamma_j} G(\vec{r}_i, \vec{r}') \mathrm{d}\Gamma'_j \right)}_{\mathcal{C}_{ij}} B_j^{\mathrm{n}}$$

$$B_i^{\tau} = \sum_j \underbrace{\left(\int_{\Gamma_j} 2\hat{\vec{e}}_{\tau} \cdot \nabla_r \frac{\partial G}{\partial n}(\vec{r}_i, \vec{r}') \mathrm{d}\Gamma'_j \right)}_{\mathcal{D}_{ij}} \Phi_j - \sum_j \underbrace{\left(\int_{\Gamma_j} 2\hat{\vec{e}}_{\tau} \cdot \nabla_r G(\vec{r}_i, \vec{r}') \mathrm{d}\Gamma'_j \right)}_{\mathcal{F}_{ij}} B_j^{n}$$

Third step: finite cylinder and kinematic code

Boundary Matrix

Matrix Equation for B^τ

$$\frac{1}{2}\Phi_i = -\mathcal{A}_{ij}\Phi_j - \mathcal{C}_{ij}B^{\mathrm{n}}_j$$

$$B^\tau_i = \mathcal{D}_{ij}\Phi_j - \mathcal{F}_{ij}B^{\mathrm{n}}_j$$

$$\mathbf{B}^\tau = \underbrace{\left(-\mathcal{D}\left(\frac{1}{2}+\mathcal{A}\right)^{-1}\mathcal{C} - \mathcal{F}\right)}_{\mathcal{H}} \cdot \mathbf{B}^n$$

- numerical computation of matrix elements with 2D-Gauss-Legendre quadrature method
- special treatment of diagonal elements (singularities) necessary

- linear, non-local expression for the tangential field components: $\mathbf{B}^\tau = \mathcal{H}\mathbf{B}^n$ where $\mathcal{H}$ is a fully occupied matrix.
- computation of B^τ_i at a single point requires the knowledge of B^n_j at every grid cell (j) at the surface.
- matrix $\mathcal{H}_{ij}$ only depends on the geometry and needs only be computed once (which, however, requires a huge amount of memory).

Third step: finite cylinder and kinematic code

Results

- Stefani *et al.*, EJMB, 2006: using MND and VKE flows, study of the influence of the walls (side and lid) $\Rightarrow$ detrimental role of (rotating) lid layers
- Laguerre *et al.*, CR Mécanique, 2006: using MND flow, with different conductivities $X = \sigma_{shell}/\sigma_{fluid} = 1$ or 5 and different (static) layers w, l (side and lid layers) $\Rightarrow$ same detrimental role of lid layers

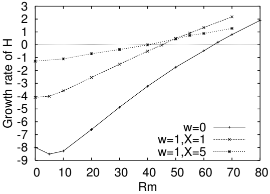

MND growthrate

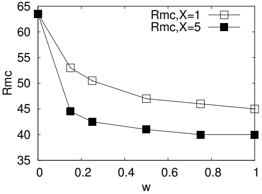

influence of w and X

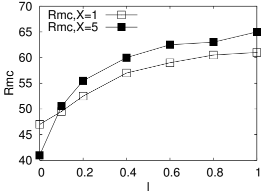

influence of l and X

- Gissinger, Iskakov *et al.*, EPL, 2008: infinite permeability BC decreases $R_{\rm mc}$
- Gissinger (EPL 2009): MND+strong non-axi vortices lead to the generation of a nearly axisymmetric dipole (but no reproducible results by COMSOL, FV-BEM nor SFEMaNS)

Fourth step: alpha-VKS in kinematic code

Mean-field induction equation using $\mathbf{B} = \mathbf{B}^{LS} + \mathbf{B}'$, $\mathbf{u} = \mathbf{u}^{LS} + \mathbf{u}'$ $\Rightarrow$

$$\partial_t \mathbf{B}^{LS} = \nabla \times (\mathbf{u}^{LS} \times \mathbf{B}^{LS} + \boldsymbol{\mathcal{E}} - \eta \nabla \times \mathbf{B}^{LS})$$

with electromotive force $\boldsymbol{\mathcal{E}} = (\mathbf{u}' \times \mathbf{B}')^{LS}$

- $\mathbf{B}^{LS}$ slightly varies around $(\mathbf{r}, t) \Rightarrow \mathcal{E}_i \approx \alpha_{ij} B_j^{LS} + \beta_{ijk} \partial_k B_j^{LS} + \ldots$
- simplest case isotropic, non-mirror symmetric turbulence: $\alpha_{ij} = \alpha \delta_{ij}$ and $\beta_{ijk} = -\eta_T \epsilon_{ijk}$ (η_T turbulent diffusivity)
- relation between α-effect and kinetic helicity: $\alpha \approx -\frac{1}{3} \tau_{corr} (\mathbf{u} \cdot \nabla \times \mathbf{u})^{LS}$
- kinematic approach with blades modeled by an $\alpha_{\theta\theta}$-effect using

$$\partial_t \mathbf{B} = \nabla \times (\widetilde{\mathbf{U}} \times \mathbf{B} + \alpha (\mathbf{B} \cdot \mathbf{e}_\theta) \mathbf{e}_\theta) - \nabla \times (\frac{1}{R_\mathrm{m}} \nabla \times \mathbf{B})$$

with $\widetilde{\mathbf{U}}$ measured VKE flow and different conductivities σ_i in the walls. Study of influence of top/bottom BC ($z = \pm H/2R_0$ and $0 \leq r \leq R_0$): vacuum (I) or perfect ferromagnetic (F)

Fourth step: alpha-VKS in kinematic code

Results

early computations by Laguerre *et al.*, PRL 2008

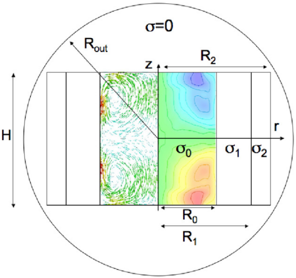

numerical domain and VKE

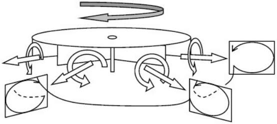

radial helical vortices between blades

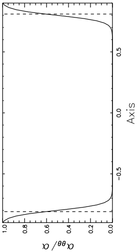

localized $\alpha_{\theta\theta}$-effect

$\Rightarrow$ good shape but irrealistic value of α-effect (numerics $\alpha \sim -30\, m\, s^{-1}$ vs rough estimate $\alpha \sim -uR_{\mathrm{m}}^{blades} = -u^2 h/\eta = -1.8\, m\, s^{-1}$ for $u_{max} \approx 15\, m\, s^{-1}$)

Fourth step: alpha-VKS in kinematic code

Results

early computations by Laguerre *et al.*, PRL 2008

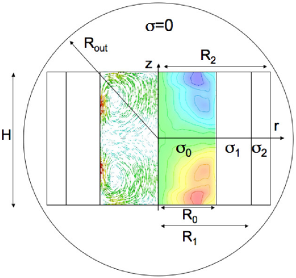

numerical domain and VKE

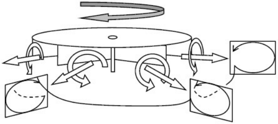

radial helical vortices between blades

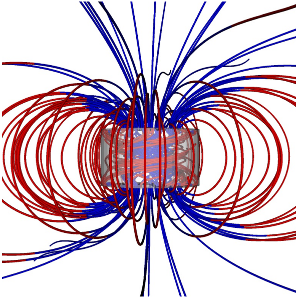

$m = 0$ (F) growing magnetic field for $R_{\rm mc} = 32$, $|\alpha| = 2.2 > |\alpha_c| = 2.1\,(\sim 30\, m\, s^{-1})$

$\Rightarrow$ good shape but irrealistic value of α-effect (numerics $\alpha \sim -30\, m\, s^{-1}$ vs rough estimate $\alpha \sim -u R_{\rm m}^{blades} = -u^2 h/\eta = -1.8\, m\, s^{-1}$ for $u_{max} \approx 15\, m\, s^{-1}$)

Fourth step: alpha-VKS in kinematic code
Results

early computations by Laguerre *et al.*, PRL 2008

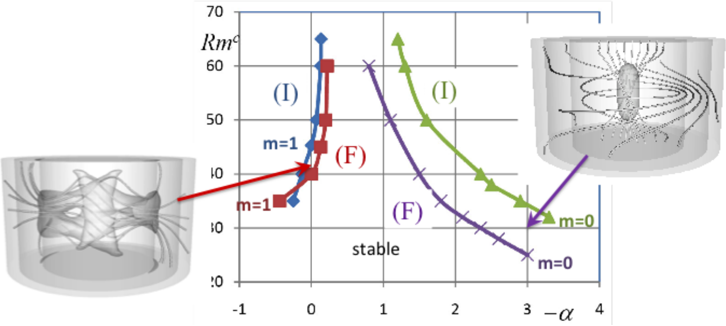

⇒ good shape but irrealistic value of α-effect (numerics $\alpha \sim -30\, m\ s^{-1}$ vs rough estimate $\alpha \sim -uR_{\mathrm{m}}^{blades} = -u^2 h/\eta = -1.8\, m\ s^{-1}$ for $u_{max} \approx 15\, m\ s^{-1}$)

Fourth step: alpha-VKS in kinematic code

Results (Giesecke, Nore *et al.*, GAFD 2010)

validation with two different codes: FV-BEM and SFEMaNS for vacuum BC

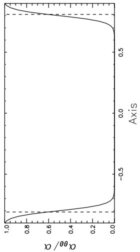

localized α-effect

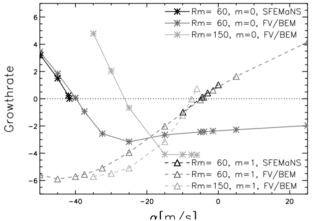

field amplitude growthrates for localized α-effect

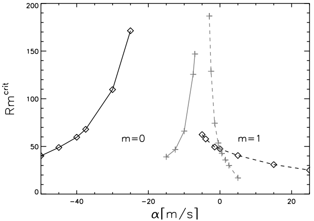

$\mathrm{Rm}^{\mathrm{crit}}$ vs α: black curves, localized α-effect; grey curves, homogenous α-effect

$\Rightarrow$ simple profiles of α need large and unrealistic values of α ($\sim -60\, m\, s^{-1}$) to explain the VKS experimental results; smaller values with homogeneous α

Fourth step: alpha-VKS in kinematic code

Results (Giesecke *et al.*, PRL 2010)

modeling of blades in kinematic code using MND flow

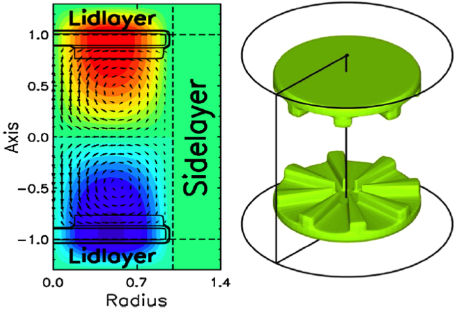

MND flow and impellers with straight blades

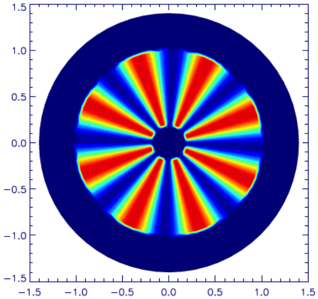

8 straight blades

Fourth step: alpha-VKS in kinematic code

Results (Giesecke *et al.*, PRL 2010)

modeling of blades in kinematic code using MND flow

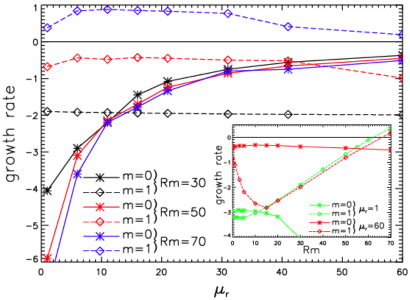

growth rates of $\mathbf{B}$ with no α-effect

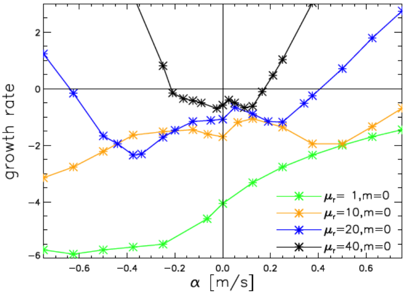

growth rates of $\mathbf{B}(m = 0)$ with homogeneous α-effect

$\Rightarrow$ no growing axisymmetric mode with $\alpha = 0$ (Cowling's thm)
$\Rightarrow$ growing $m = 0$ mode if very small α is included: efficient interaction of α with μ_r within the impeller region

Fourth step: alpha-VKS in kinematic code

Results (Giesecke *et al.*, PRL 2010)

modeling of blades in kinematic code using MND flow

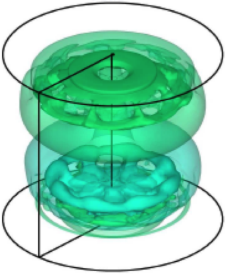

density plot of magnetic energy with small α

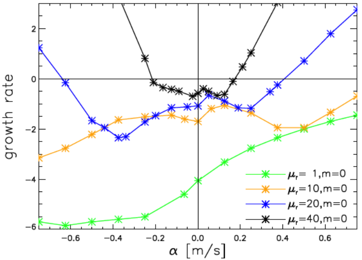

growth rates of $\mathbf{B}(m=0)$ with homogeneous α-effect

$\Rightarrow$ no growing axisymmetric mode with $\alpha = 0$ (Cowling's thm)

$\Rightarrow$ growing $m = 0$ mode if very small α is included: efficient interaction of α with μ_r within the impeller region

$\Rightarrow$ good shape but homogeneous α-effect not really realistic

Fifth step: Direct Numerical Simulation

The non-dimensionalised MHD equations:

- Navier-Stokes equations for an incompressible fluid:
$$\begin{aligned} \partial_t \mathbf{u} + \mathbf{u}\cdot\nabla\mathbf{u} - \frac{1}{R_e}\Delta\mathbf{u} + \nabla p &= (\nabla\times\frac{\mathbf{B}}{\mu_r})\times\mathbf{B} + \mathbf{f}, \\ \nabla\cdot\mathbf{u} &= 0. \end{aligned}$$
- Maxwell equations for the induction field $\mathbf{B}$ (magnetic field $\mathbf{H} = \mathbf{B}/\mu_r$):
$$\begin{aligned} \partial_t \mathbf{B} &= -\frac{1}{R_\mathrm{m}}\nabla\times\left(\frac{1}{\sigma_r}\nabla\times\frac{\mathbf{B}}{\mu_r}\right) + \nabla\times(\mathbf{u}\times\mathbf{B}), \\ \nabla\cdot\mathbf{B} &= 0. \end{aligned}$$
- Kinetic and magnetic Reynolds numbers with ν kinematic viscosity, μ_0 vacuum magnetic permeability, σ_0 fluid electrical conductivity (and magnetic Prandtl number):

$$R_e = \frac{U_{\mathrm{ref}} L_{\mathrm{ref}}}{\nu}, \qquad R_\mathrm{m} = \mu_0\sigma_0 U_{\mathrm{ref}} L_{\mathrm{ref}}, \qquad P_m = \frac{R_\mathrm{m}}{R_\mathrm{e}} = \mu_0\sigma_0\nu.$$

SFEMaNS code from 2002 to now

Code developed by J.-L. Guermond, myself, PhD students and post-docs since 2002 (R. Laguerre, A. Ribeiro, K. Boronska, F. Luddens, D. Castanon-Quiroz and L. Cappanera)

Basics

- Axisymmetric geometry
- Fourier decomposition in the azimuthal direction
- Lagrange finite elements in the meridian plane ($\mathbb{P}_1$-$\mathbb{P}_2$ polynoms)

Code capabilities

- Hydrodynamic, thermal convection, magnetic and MHD studies
- Description of vacuum
- Permeability and conductivity jumps (in radial and axial directions)
- Parallelization with respect to Fourier modes and domain decomposition in the meridian plane
- Entropy viscosity method-LES to reach higher R_e (Guermond *et al.*, 2008)
- Pseudo-penalty method to impose obstacles (Pasquetti *et al.*, ANM 2008)

Scheme of SFEMaNS

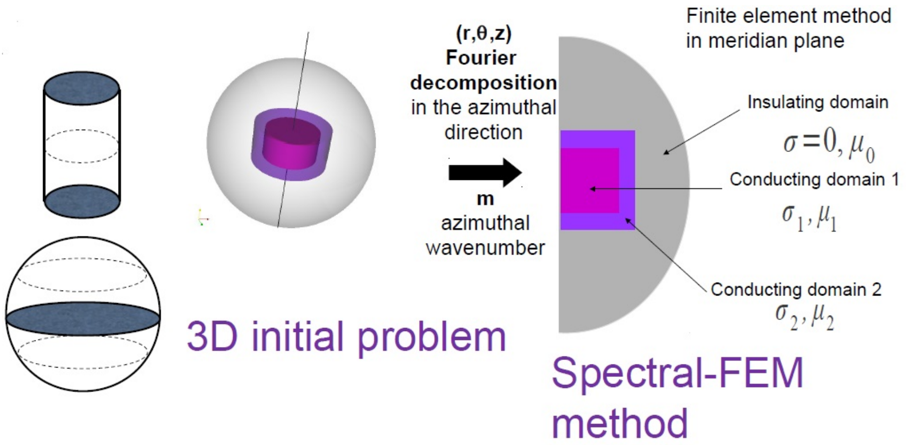

Figure : SFEMaNS using $f(r,\theta,z,t) = \sum_{m=0}^{M} f_m^c(r,z,t)\cos m\theta + \sum_{m=1}^{M} f_m^s(r,z,t)\sin m\theta$ and $f_m^c(r,z,t)$ approximation in F.E. space ($\mathbb{P}_1$-$\mathbb{P}_2$ polynoms)

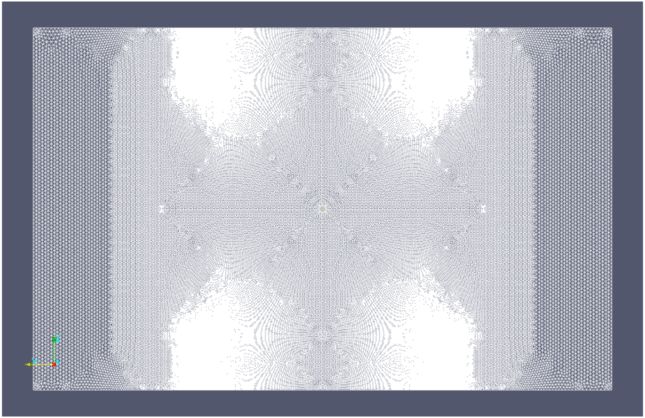

Figure : Meridian mesh with finite elements ($h_{wall} = 0.01$ and $h_{\text{blades}} = 0.0025$)

Magnetic domain with different regions: $\Omega = \{(r, \theta, z) \in [0, 1] \times [0, 2\pi) \times [-1, 1]\}$ for fluid and $\Omega_{\text{out}} = \{(r, \theta, z) \in [1, 1.6] \times [0, 2\pi) \times [-1, 1]\}$ for the stagnant sodium layer and the copper outer wall

Impellers in SFEMaNS using a pseudo-penalty method

Pseudo-penalty (Pasquetti *et al.*, Appl. Num. Math., **58**, 2008)

$$\frac{\mathbf{u}^{n+1} - \chi \mathbf{u}^n}{\tau} - R_e^{-1} \Delta \mathbf{u}^{n+1} + \nabla p^{n+1} = \chi \mathbf{f}^{n+1},$$
$$\nabla \cdot \mathbf{u}^{n+1} = 0,$$

with χ penalty function (1 in fluid, 0 in solid)

- One mesh and order 1 in time method (error in τR_e^{-1})
- Nonlinear terms from pseudo-penalty explicitly treated
- Adaptation to a predictor-corrector scheme (penalty on pressure increments)
- Extension to moving solid obstacles with speed $\mathbf{u}_{\mathrm{obs}}$
- Ferromagnetic moving impellers treated as varying relative permeability zones with $1 \leq \mu_r(r, \theta, z, t) \leq \mu_{max}$

Navier-Stokes scheme

$$\frac{\mathbf{u}^{n+1} - \chi^{n+1}\mathbf{u}^n}{\tau} - \frac{1}{R_e}\Delta\mathbf{u}^{n+1} = -\nabla p^n + \chi^{n+1}\left(-(\nabla\times\mathbf{u}^n)\times\mathbf{u}^n - \nabla\psi^n\right) + (1-\chi^{n+1})\frac{\mathbf{u}_{\text{obst}}^{n+1}}{\tau},$$

with χ penalty function (1 in fluid, 0 in solid) and $\nabla\cdot\mathbf{u}^{n+1} = 0$

Maxwell scheme

$$\frac{\mathbf{B}^{n+1} - \mathbf{B}^n}{\tau} + \frac{1}{R_\mathrm{m}}\nabla\times\left[\frac{1}{\sigma_r}\nabla\times\left(\frac{\mathbf{B}^{n+1} - \mathbf{B}^n}{\overline{\mu}}\right)\right] = -\frac{1}{R_\mathrm{m}}\nabla\times\left[\frac{1}{\sigma_r}\left(\nabla\times\frac{\mathbf{B}^n}{\mu_r^n}\right)\right] + \nabla\times(\mathbf{u}^{n+1}\times\mathbf{B}^n)$$

with τ timestep, σ_r relative conductivity, $\overline{\mu} \leq \mu_r$ and $R_m = \mu_0\sigma_0 U_{\text{ref}} L_{\text{ref}}$

Von Kármán flow

Experimental set-up

- Metal impellers TM73 used by VKS2 (Monchaux *et al.* 2007)
- 8 blades on each disk with $R_{imp}/R_{cyl} = 0.75$
- Curvature angle of 24^o
- Counter-rotating impellers
- Unscooping sense ("dos cuillère")

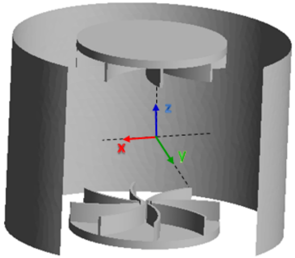

Numerical study of the hydrodynamic regime

- Control parameter $R_e = R^2_{\mathrm{cyl}}\omega/\nu$
- DNS with 128 or 192 Fourier modes and
- non-uniform meridian mesh ($h_{wall} = 0.01$ and $h_{\mathrm{blades}} = 0.0025$)

Hydrodynamic regime for $500 \leq R_e \leq 2500$

- Unsteady flow
- Breaking of axisymmetry
- $m = 2$ mode predominant for $R_e = 500$
- $m = 3$ mode predominant for $R_e \geq 675 \longrightarrow$ **all u modes** coupled

- Fluid exchange between upper & lower parts at $R_e = 500$

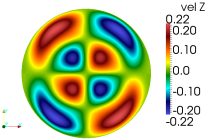

Helical vortices between blades (Ravelet *et al.* 2012, Kreuzahler *et al.* 2014)

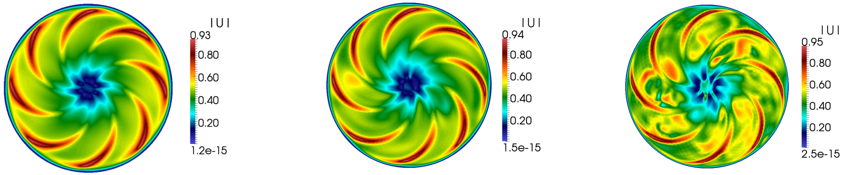

$R_e = 500$ $R_e = 1000$ $R_e = 2500$

Figure : $|\mathbf{u}|$ near bottom impeller

Hydrodynamic regime for $200 \leq R_e \leq 2500$

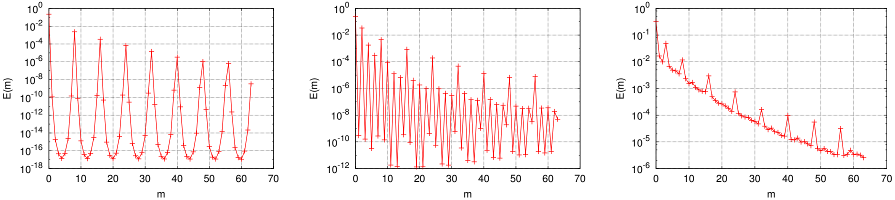

$R_e = 200$ $\quad$ $R_e = 500$ $\quad$ $R_e = 2500$

Figure : Time averaged spectra of the kinetic energy as a function of the azimuthal mode

- for $R_e < 500$ only $m = 0$ and 8 (and harmonics) are populated
- at $R_e = 500$, $m = 0$ and 2 in $\mathbf{u}$ dominate $\longrightarrow$ splitting between even $\mathbf{H}$ family [0-family] and odd $\mathbf{H}$ family [1-family] (via EMF $\mathbf{u} \times \mathbf{B}$)
- for $R_e > 800$, all $\mathbf{u}$ modes are coupled $\longrightarrow$ no splitting for $\mathbf{H}$

MHD regime

Experimental set-up

- Metal impellers TM73 used by VKS2 (Monchaux *et al.* 2007)
- 8 blades on each disk with $R_{imp}/R_{cyl} = 0.75$
- Curvature angle of 24^o
- Counter-rotating impellers
- Unscooping sense ("dos cuillère")

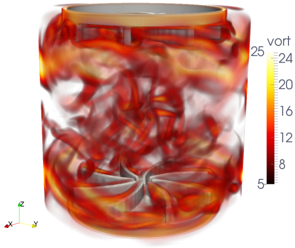

Figure : $R_e = 2500$, $|\nabla \times \mathbf{u}|$

Numerical study of the MHD regime at $R_e = R_{cyl}^2 \omega/\nu = 500$ and 1500 with $R_\mathrm{m} = \mu_0 \sigma_0 R_{cyl}^2 \omega$

- at $R_e = 500$, $m = 0$ and 2 in $\mathbf{u}$ dominate $\longrightarrow$ splitting between even $\mathbf{H}$ family [0-family] and odd $\mathbf{H}$ family [1-family] (via EMF $\mathbf{u} \times \mathbf{B}$)
- at $R_e = 1500$, all $\mathbf{u}$ modes are coupled $\longrightarrow$ no splitting for $\mathbf{H}$

MHD regime at $R_e = 500$

- Onset of dynamo action monitored by the total magnetic energy, $M(t) = \frac{1}{2}\int_\Omega \mathbf{H}(\mathbf{r},t)\cdot\mathbf{B}(\mathbf{r},t)d\mathbf{r}$, as well as the modal energies $M_m(t) = \int_\Omega \frac{1}{2}|\hat{\mathbf{H}}(r,m,z,t)|^2 \mathrm{d}r\mathrm{d}z$
- Linear dynamo action $M(t) \approx \exp((\lambda_r + i\lambda_i)t)$ with $\lambda_r > 0$
- Nonlinear dynamo action when $M(t)$ saturates
- Variation of the relative permeability of impellers μ_r

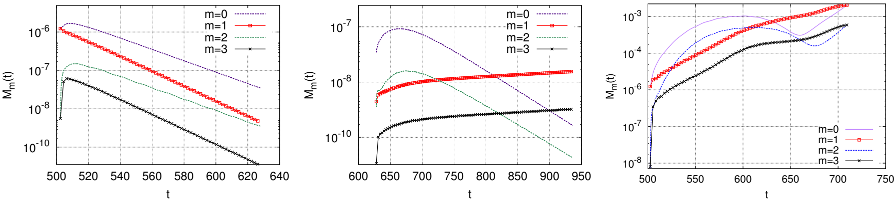

$R_\mathrm{m} = 50$ $R_\mathrm{m} = 150$ $R_\mathrm{m} = 300$

Figure : $M_m(t)$ for $m = 0, 1, 2, 3$ and for $R_\mathrm{m} \in [50, 300]$ at $R_e = 500$ and $\mu_r = 5$

MHD regime at $R_e = 500$

- Onset of dynamo action monitored by the total magnetic energy, $M(t) = \frac{1}{2}\int_\Omega \mathbf{H}(\mathbf{r},t)\cdot\mathbf{B}(\mathbf{r},t)d\mathbf{r}$, as well as the modal energies $M_m(t) = \int_\Omega \frac{1}{2}|\hat{\mathbf{H}}(r,m,z,t)|^2 \mathrm{d}r\mathrm{d}z$
- Linear dynamo action $M(t) \approx \exp((\lambda_r + i\lambda_i)t)$ with $\lambda_r > 0$
- Nonlinear dynamo action when $M(t)$ saturates
- Variation of the relative permeability of impellers μ_r

μ_r	$R_{\rm m}^c$(0-family)	$R_{\rm m}^c$(1-family)	P_m^c(0-family)	P_m^c(1-family)
5	240 $\pm$5	147 $\pm$1	0.48	0.29
50	130 $\pm$2	138 $\pm$2	0.26	0.28
100	82 $\pm$2	144 $\pm$2	0.16	0.29

Table : Magnetic thresholds for $R_e = 500$

MHD regime at $R_e = 500$

- Onset of dynamo action monitored by the total magnetic energy, $M(t) = \frac{1}{2}\int_\Omega \mathbf{H}(\mathbf{r},t)\cdot\mathbf{B}(\mathbf{r},t)d\mathbf{r}$, as well as the modal energies $M_m(t) = \int_\Omega \frac{1}{2}|\hat{\mathbf{H}}(r,m,z,t)|^2 \mathrm{d}r\mathrm{d}z$
- Linear dynamo action $M(t) \approx \exp((\lambda_r + i\lambda_i)t)$ with $\lambda_r > 0$
- Nonlinear dynamo action when $M(t)$ saturates
- Variation of the relative permeability of impellers μ_r

μ_r	R^c_{m}(0-family)	R^c_{m}(1-family)	P^c_m(0-family)	P^c_m(1-family)
5	240 $\pm$5	147 $\pm$1	0.48	0.29
50	130 $\pm$2	138 $\pm$2	0.26	0.28
100	82 $\pm$2	144 $\pm$2	0.16	0.29

Table : Magnetic thresholds for $R_e = 500$

- 1-family thresholds non sensitive to $\mu_r \rightarrow$ bulk mode
- 0-family thresholds very sensitive to $\mu_r \rightarrow$ ferromagnetic impellers are crucial

MHD regime at $R_e = 500$

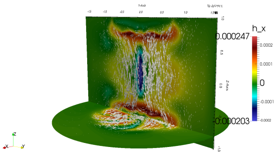

$\mu_r = 5$, 1-family

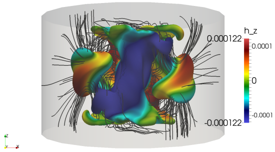

$\mu_r = 5$, 1-family

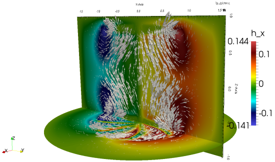

$\mu_r = 100$, 0-family

Figure : MHD simulations at $R_e = 500$, $R_\mathrm{m} = 150$ and (a-b) $\mu_r = 5$ (1-family, **equatorial dipole and 2 vertical structures**), (c) $\mu_r = 100$ (0-family, **axial dipole)**

MHD regime at $R_e = 500$, $R_\mathrm{m} = 100$ and $\mu_r = 100$

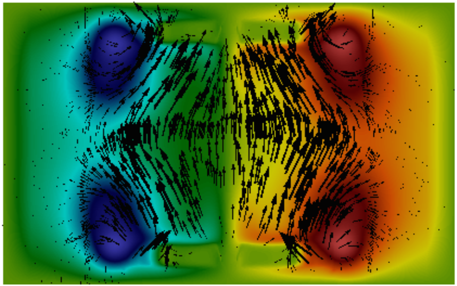

(H_y, H_z) vector field, H_x color

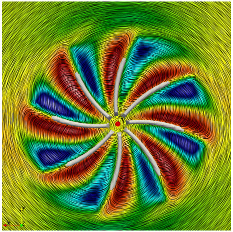

H_z at $z = 0.8$

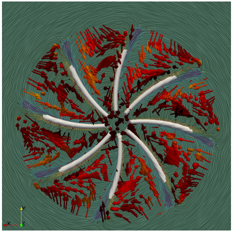

B_z and $\mathbf{j}$ at $z = 0.8$ (top blade seen from bottom)

- axial dipole and toroidal H_θ similar to experimental magnetic field
- H_z located between blades, B_z concentrated in blades

MHD regime at $R_e = 1500$

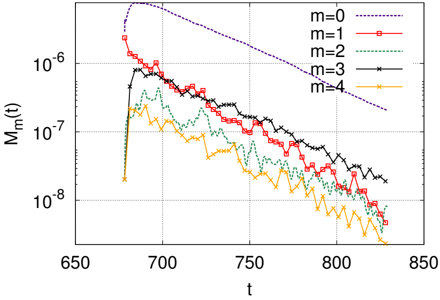

$R_\mathrm{m} = 50$

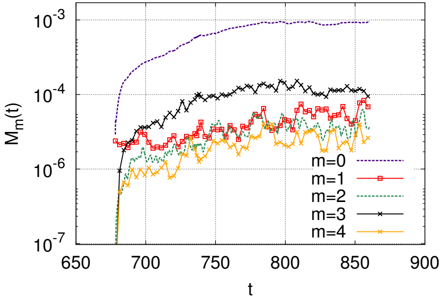

$R_\mathrm{m} = 100$

Figure : $M_m(t)$ for $m \in [0, 4]$ and for $R_\mathrm{m} \in \{50, 100\}$ at $R_e = 1500$ and $\mu_r = 50$

- all **H** modes are coupled (same slope in linear regime)

MHD regime at $R_e = 1500$

μ_r	R_{m}^c	P_m^c
5	150 ± 5	0.10
50	90 ± 5	0.06

Table : Magnetic thresholds for $R_e = 1500$

MHD regime at $R_e = 1500$

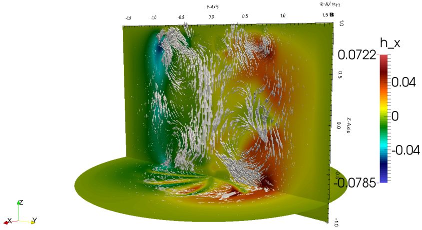

Instantaneous magnetic field

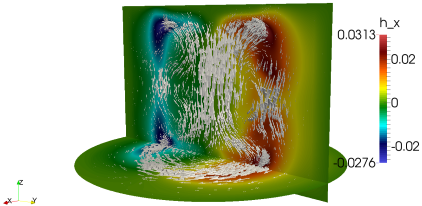

Time averaged magnetic field

Figure : MHD simulations at $R_e = 1500$, $R_\mathrm{m} = 150$ and $\mu_r = 50$, dominated by an **axisymmetric axial dipole**

MHD regime in the TM73 VKS configuration at $R_e = 1500$, $R_\mathrm{m} = 150$ and $\mu_r = 50$

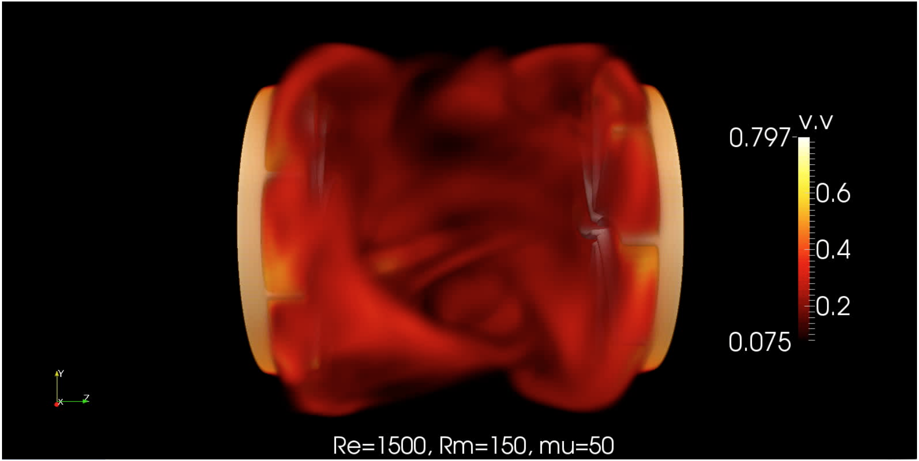

MHD regime in the TM73 VKS configuration at $R_e = 1500$, $R_{\mathrm{m}} = 150$ and $\mu_r = 50$

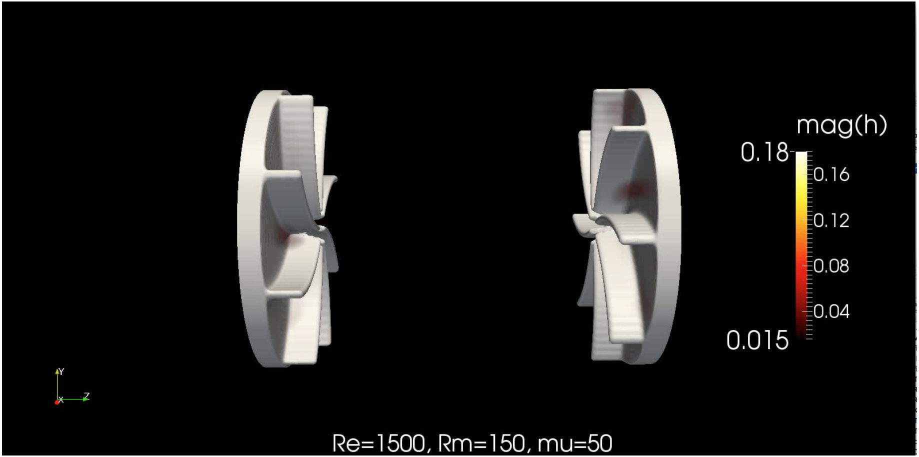

Speculative mechanism

A solid-fluid mechanism

- The Ω-effect due to the rotating impellers generates a toroidal/azimuthal magnetic field from poloidal/axial magnetic field seeds;
- This azimuthal magnetic field is **stored** in the high permeability disk;
- It is then collected in the blades and collimated into a poloidal field by the helical vortices (α-effect).

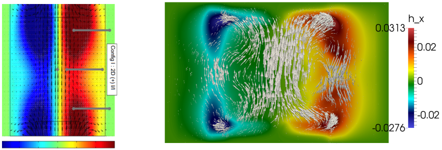

Exp. **H** Num. **H**

Figure : Good agreement between experimental (Boisson *et al.* 2012) and numerical results

Speculative mechanism

A solid-fluid mechanism

- The Ω-effect due to the rotating impellers generates a toroidal/azimuthal magnetic field from poloidal/axial magnetic field seeds;
- This azimuthal magnetic field is **stored** in the high permeability disk;
- It is then collected in the blades and collimated into a poloidal field by the helical vortices (α-effect).

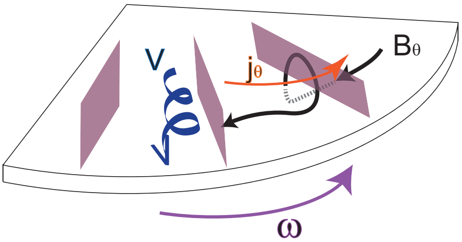

Figure : $\alpha - \Omega$ mechanism **(Pétrélis *et al.*, GAFD 2007, Laguerre *et al.*, PRL 2008)**

Conclusion for dynamo action in VKS

μ_r	R_{m}^c(0-family)	R_{m}^c(1-family)
5	240 ± 5	147 ± 1
50	130 ± 2	138 ± 2
100	82 ± 2	144 ± 2

Table : Magnetic thresholds for $R_e = 500$

μ_r	R_{m}^c
5	150 ± 5
50	90 ± 5

Table : Magnetic thresholds for $R_e = 1500$

- Ferromagnetic impellers enhance axisymmetric magnetic field
- Increasing R_e lowers the dynamo threshold R_{m}^c
- Speculative mechanism (similar to Yannick Ponty's one)
- R_{m}^c(VKS) ≈ 55 at $R_e \approx 10^7$ with soft iron impellers $\mu_r \approx 60$!

Conclusion for dynamo action in VKS

μ_r	R_m^c(0-family)	R_m^c(1-family)
5	240 $\pm$5	147 $\pm$1
50	130 $\pm$2	138 $\pm$2
100	82 $\pm$2	144 $\pm$2

Table : Magnetic thresholds for $R_e = 500$

μ_r	R_m^c
5	150 $\pm$5
50	90 $\pm$5

Table : Magnetic thresholds for $R_e = 1500$

- Ferromagnetic impellers enhance axisymmetric magnetic field
- Increasing R_e lowers the dynamo threshold R_m^c
- Speculative mechanism (similar to Yannick Ponty's one)
- R_m^c(VKS) ≈ 55 at $R_e \approx 10^7$ with soft iron impellers $\mu_r \approx 60$!

Future work

- Study higher R_e numbers in Von Kármán flows to compare with experiments (CEA Saclay, Dubrulle *et al.*)
- $R_m^c \to$ constant as $R_e \to \infty$?

Outline

Conclusion

- topic of Numerical dynamos is large (my talk is not exhaustive!) and active
- what next?
  - optimization of kinematic dynamos **(Chen *et al.*, JFM 2015, Herreman, JFM 2016)**
  - reach high R_e using LES models $\Rightarrow$ question about super/subcriticality bifurcation with decreasing P_m
  - scale separation for optimizing $P_{\mathrm{ref}} = PL/\rho\eta^3 \propto R_{\mathrm{m}}^3 L/l_f$ **(Sadek *et al.*, PRL 2016)**
  - wait for the new dynamo experiment in Dresden using a precessing cylinder

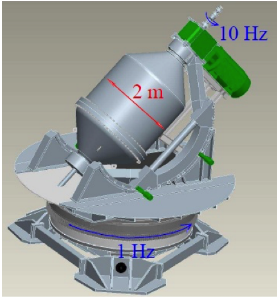

Dresdyn cylinder

Axial spin: vorticity streamlines in red, **B** in yellow/green

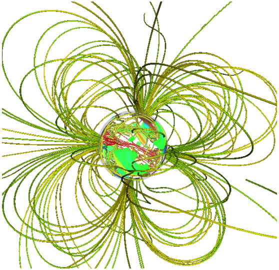

$R_e = 1200$, $R_{\mathrm{m}} = 2400 > R_{\mathrm{mc}} \approx 775$

Thank you for your attention